J. Fluid Mech. (1998), *vol.* 363, *pp.* 301–323. Printed in the United Kingdom

The background flow method. Part 2. Asymptotic theory of dissipation bounds

By ROLF NICODEMUS, S. GROSSMANN AND M. HOLTHAUS

Fachbereich Physik der Philipps-Universität, Renthof 6, D–35032 Marburg, Germany

(Received 11 August 1997 and in revised form 8 December 1997)

We study analytically the asymptotics of the upper bound on energy dissipation for the two-dimensional plane Couette flow considered numerically in Part 1 of this work, in order to identify the mechanisms underlying the variational approach. With the help of shape functions that specify the variational profiles either in the interior or in the boundary layers, it becomes possible to quantitatively explain all numerically observed features, from the occurrence of two branches of minimizing wavenumbers to the asymptotic parameter scaling with the Reynolds number. In addition, we derive a new variational principle for the asymptotic bound on the dissipation rate. The analysis of this principle reveals that the best possible bound can only be attained if the variational profiles allow the shape of the boundary layers to change with increasing Reynolds number.

1. Introduction

The numerical exploration of the extended Doering–Constantin variational principle (Doering & Constantin 1994; Nicodemus, Grossmann & Holthaus 1997*a*) for computing bounds on the rate of energy dissipation in turbulent shear flow, as reported in Part 1 of this work (Nicodemus, Grossmann & Holthaus 1998), has revealed some fairly systematic features: at a certain Reynolds number the minimizing wavenumbers bifurcate, such that the optimal upper bound on the dissipation rate is determined by both minima simultaneously. Moreover, the optimized parameters of the variational profiles exhibit a simple scaling behaviour. These findings call for an analytical explanation.

In the present second part of our study we will develop a detailed asymptotic theory for the model problem considered in Part 1, the plane Couette flow without spanwise degrees of freedom. From the numerical solution of the variational problem for the unrestricted, three-dimensional Couette problem (Nicodemus, Grossmann & Holthaus 1997*b*) we know that this model actually captures all relevant facts.

The plan of our analysis is the following: in § 2 we study the two minimizing wavenumber branches on the basis of the spectral constraint. The most important technical tools introduced there are two types of *shape functions*, which are not variational profiles themselves, but which contain the essential information about the profiles either in the interior or in the boundary layers. These functions will allow us to show that in the asymptotic regime one of the minimizing wavenumbers is determined solely by the shape of the profiles in the interior, the other one solely by the shape of the profiles in their boundary layers. We build our arguments mainly

on two lemmas, which have been formulated such that the propositions are as mild as possible, but which will be found to have far-reaching implications. Together with a third, more technical lemma which has been banished to the Appendix, they will allow us to understand the asymptotics of the two minimizing wavenumbers.

An understanding of the two minimizing wavenumbers, however, does not automatically imply an understanding of the optimal upper bound on the dissipation rate, since the two minima of $R_0\{\phi\}(k)$ (see (3.30) in Part 1) might have different values, and it is only the global minimum that matters for the variational principle. The astonishing observation that both minima actually take on the same value is explained in § 3. It will be shown that, besides the characterization of the profiles by two shape functions, only a certain monotonic property is required to prove both the locking of the two minima to the same value and the *Re*-scaling behaviour of the optimal profile parameters; it will even be possible to express the power law prefactors in terms of the shape functions.

The next step then is to show in § 4 that the optimal asymptotic upper bound of the dissipation rate is determined entirely by the behaviour of the variational profiles in the boundary layers, and to formulate a much simpler variational principle for this asymptotic bound. The solution of this new principle will reveal that the best bounds derivable from the extended Doering–Constantin principle can be obtained only if the variational profiles contain a parameter which governs their shape within the boundary layers. This insight will be taken up in § 5 in order to compute the upper bound with the help of such a generalized class of test profiles for all Reynolds numbers, resulting in the bound that has already been included in the overview given in figure 9 of Part 1.

Finally, we will draw our conclusions in § 6. When referring to a formula from Part 1, this will be indicated by the roman numeral I followed by the equation number.

2. The two branches of the bifurcation plot

Let us recall a key result obtained in the numerical solution of the variational principle (I, 2.12) with the spectral constraint (I, 2.13) for the restricted plane Couette flow: for Reynolds numbers above $Re_B \approx 860$ the critical Reynolds number $R_c\{\phi\}$, up to which a given profile ϕ remains an admissible test function, is associated with two different wavenumbers k_1 and k_2. This implies a degeneracy of the eigenvalue problem (I, 2.13): two eigenvalues pass through zero simultaneously. After optimization over all profiles, one of these two k-branches scales linearly with Re, the other becomes constant. The two branches of minimizing wavenumbers resulting from a particular choice of test profiles have been depicted in figure 7 of Part 1, which will be referred to as *bifurcation plot* in the following. In this section we explain the emergence of the two branches analytically.

The starting point is the boundary value problem (I, 4.3)–(I, 4.8), which arises in the reformulation of the spectral constraint:

$$y_1' = 2k\,[-y_1 + y_2]\,, \tag{2.1}$$

$$y_2' = 2k\left[\tfrac{1}{2}y_1 - y_2 + \tfrac{1}{2}y_4\right], \tag{2.2}$$

$$y_3' = -2ky_3 - \frac{R}{k}\,\phi' y_1, \tag{2.3}$$

$$y_4' = 2k\,[-y_4 + y_5]\,, \tag{2.4}$$

$$y_5' = 2k\left[\tfrac{1}{4}y_1 + \tfrac{1}{2}y_4 - y_5 + \tfrac{1}{4}y_6\right], \tag{2.5}$$

$$y_6' = 2k\,[y_2 - y_6] + \frac{R}{2k}\,\phi' y_3 \tag{2.6}$$

with initial condition

$$\boldsymbol{y}(0) = (0,0,0,0,0,1)^T \tag{2.7}$$

and boundary condition

$$y_1(1) = 0. \tag{2.8}$$

R is the rescaled Reynolds number, see (I, 2.14), $k > 0$ the absolute value of the wavenumber pertaining to the x-direction, and $\phi(z)$ is some profile function. We will denote these quantities as the *input* to the system (2.1)–(2.6). The equivalence of this boundary value problem to the spectral constraint (I, 2.13) has been established in §§ 3 and 4 of Part 1. Our goal here is to elucidate how the magnitude of the wavenumber k determines the sensitivity of this problem to the shape of the profiles ϕ. Namely, if we have profiles with boundary segments of thickness δ, see (I, 4.1) for a specific example, and if we keep k fixed while letting δ tend to zero, then the above boundary value problem becomes sensitive solely to the shape of the profiles in the interior, whereas it is solely the shape of the boundary segments that becomes essential if we take k proportional to δ^{-1}.

Thus, in the following we consider quite general families of profile functions ϕ_δ parametrized by the width δ of their boundary segments, $0 < \delta < \frac{1}{2}$. Each profile can be divided into three parts, corresponding to the intervals $0 \leqslant z \leqslant \delta$ ('left-hand boundary layer'), $\delta \leqslant z \leqslant 1-\delta$ ('interior') and $1-\delta \leqslant z \leqslant 1$ ('right-hand boundary layer'). Rather than focusing directly on the Reynolds number, we use δ as the control parameter. The limit of interest is $\delta \to 0$; different powers of $1/\delta$ characterize different orders of magnitude.

2.1. *Wavenumbers of $O(\delta^0)$: the lower branch*

If the wavenumber k entering the problem (2.1)–(2.6) is kept (almost) fixed while the profiles, and hence δ, are varied, we have

$$k = O(\delta^0) \quad \text{and} \quad k^{-1} = O(\delta^0). \tag{2.9}$$

It will be useful to introduce functions $\psi(z)$ which, although they are not variational profiles themselves, contain information about the shape of the actual profile functions $\phi(z)$. Their purpose will become clear from the following lemma:

LEMMA 2.1. *Let $\psi(z)$ be some continuously differentiable function defined in the interval* $[0,1]$ *which satisfies the equation*

$$\psi'\left(\tfrac{1}{2}\right) = 1, \tag{2.10}$$

and let R_ψ be a positive constant. In addition, let $\phi_\delta(z)$ be a family of continuously differentiable functions defined in $[0,1]$ *which are parametrized by δ, $0 < \delta < \frac{1}{2}$, and also depend continuously on some additional parameter $p_\delta > 0$. Assume further that the following properties hold:*

(i) *ϕ_δ and p_δ depend continuously on the parameter δ;*

(ii) *for each δ the function ϕ_δ in the interior is determined by ψ according to*

$$\phi_\delta'(z) = p_\delta\,\psi'(z) \quad \textit{for} \quad \delta < z < 1-\delta; \tag{2.11}$$

(iii) *within the boundary layers, i.e. for $0 \leqslant z \leqslant \delta$ and $1-\delta \leqslant z \leqslant 1$, one has*

$$\phi_\delta'(z) = p_\delta \times O(\delta^{-5/2}). \tag{2.12}$$

Then it follows that the first component of the solution vector $\mathbf{y}_\psi$ *originating from the initial value problem (2.1)–(2.7) with input quantities* k, $R = R_\psi$, *and* $\phi(z) = \psi(z)$ *differs from the first component of the solution vector* $\mathbf{y}_\delta$ *corresponding to the input* k, $R = R_\psi / p_\delta$, *and* $\phi(z) = \phi_\delta(z)$ *in the entire interval* $[0,1]$ *at most by an amount of* $O(\delta)$,

$$y_{\delta,1}(z) = y_{\psi,1}(z) + O(\delta)\,. \tag{2.13}$$

Proof. After rewriting the initial value problem (2.1)–(2.7) as an equivalent vector integral equation, one can make in each of the three regimes $0 \leqslant z \leqslant \delta$, $\delta \leqslant z \leqslant 1-\delta$, and $1-\delta \leqslant z \leqslant 1$ an ansatz of the form

$$y_{\delta,i}(z) = y_{\psi,i}(z) + O(\delta^{\alpha_i}), \quad i = 1,\ldots,6.$$

Employing the properties (2.9), (2.11), and (2.12), one can fix the exponents α_i and show by means of integral estimates that one indeed has obtained a solution within each interval. Gluing the three parts of the solution together, one finds a solution in the entire interval $[0,1]$ which satisfies (2.13). The statement then follows from the fact that the solution to the initial value problem is unique. □

Note the spirit of this lemma: the reference function $\psi(z)$ is not a profile, since it does not have to satisfy the profiles' boundary conditions, but it is used nonetheless as an input for the initial value problem. Even though the derivative of $\phi_\delta(z)$ is not related to that of $\psi(z)$ within the boundary layers, the difference of the first components of the corresponding solution vectors remains small. Because of the normalization (2.10) the parameter p_δ is the slope of ϕ_δ at $z = \frac{1}{2}$. Thus, p_δ can be considered as a generalization of the parameter p employed previously in (I, 4.1).

In order to make the lemma work we now introduce *shape functions for the interior*, i.e. functions $\psi_{int}(z)$ which are continuously differentiable in $[0,1]$, fulfil the requirement

$$\psi'_{int}\left(\tfrac{1}{2}\right) = 1 \tag{2.14}$$

and the additional symmetry condition

$$\psi'_{int}(z) = \psi'_{int}(1-z)\,. \tag{2.15}$$

We then take a fixed k together with ψ_{int} as input to the system (2.1)–(2.6), and set R_ψ to the smallest positive R-value for which the boundary value problem (2.1)–(2.8) is satisfied, $R_\psi = R_0\{\psi_{int}\}(k)$, generalizing the notation introduced in § 3 of Part 1. If we now restrict the family $\phi_\delta(z)$ to functions with the properties

$$\phi_\delta(0) = 0, \quad \phi_\delta(1) = 1, \quad \text{and} \quad \phi_\delta(z) = 1 - \phi_\delta(1-z)\,, \tag{2.16}$$

so that each ϕ_δ becomes a candidate profile for the variational principle, see (I, 2.10)–(I, 2.13), then the statement (2.13) of the lemma, applied in the limit $\delta \to 0$, asserts

$$\lim_{\delta\to 0} p_\delta\, R_0\{\phi_\delta\}(k) = R_0\{\psi_{int}\}(k)\,, \tag{2.17}$$

with p_δ denoting the slope of ϕ_δ at $z = \frac{1}{2}$. Moreover, considering $R_0\{\psi_{int}\}(k)$ as a function of the wavenumber k, this function will exhibit a global minimum for some $k > 0$. By construction, the minimizing wavenumber does not depend on the boundary layer thickness δ, and therefore is of the required order, $O\left(\delta^0\right)$. The equation (2.17) thus states that for sufficiently small δ the minima corresponding to the actual profiles ϕ_δ can be understood in terms of a shape function that specifies the profiles in the interior only.

Hence, for families of profiles ϕ_δ that merely possess the 'weak' properties (2.16), (2.11), and (2.12), we have obtained a rather strong statement: *for small δ, and provided k is of $O(\delta^0)$, the k-dependencies of $R_0\{\phi_\delta\}(k)$ are mirror images of the k-dependence of $R_0\{\psi_{int}\}(k)$, where the function $\psi_{int}(z)$ contains the information about the shape of the profiles ϕ_δ in the interior*. This implies that for small δ the behaviour of the profiles within the boundary layers plays no role, if k is kept constant.

Focusing now on the minima

$$R_1\{\phi_\delta\} \equiv \min_{k=O(\delta^0)} \{R_0\{\phi_\delta\}(k)\}, \tag{2.18}$$

we obtain from (2.17) that

$$\lim_{\delta\to 0} p_\delta \, R_1\{\phi_\delta\} = R_c\{\psi_{int}\} \tag{2.19}$$

with $R_c\{\psi_{int}\} \equiv \min_{k>0} \{R_0\{\psi_{int}\}(k)\}$. The minimizing k will be denoted as $k_c\{\psi_{int}\}$.

We can harvest the first fruits of this abstract reasoning when we apply these arguments to the profile functions (I, 4.1), which have been employed for the numerical analysis in Part 1 of this work. Here the parameter p_δ equals the previous p, and a corresponding shape function for the interior – uniquely determined up to a constant – is just the laminar profile,

$$\psi_{int}(z) = z. \tag{2.20}$$

If we take the scaling properties (I, 5.4) for δ and p for granted, $\delta \sim \alpha Re^{-1}$, $p \sim \beta Re^{-1}$, – this gap will be closed later – then we have within the two boundary layers $p^{-1}\phi'(z) = O(\delta^{-1})\,[p + O(\delta^{-1})] = O(\delta^{-2})$. Thus, with $R_\psi = R_0\{\psi_{int}(z) = z\}(k)$ and $p_\delta = p$ the condition (2.12) of the lemma is satisfied, so that we now understand why the lower k-branch of the bifurcation plot, denoted as k_1, approaches for $Re \to \infty$ the very same k-value that also characterizes the energy stability limit Re_{ES}: since the laminar profile serves as a shape function in the limit of high Reynolds numbers, so that the ensuing high-Re minima pertaining to k_1 are replicas of the minima at the energy stability limit, we have the exact identity (with the number in brackets denoting the uncertainty of the last digit)

$$\lim_{Re\to\infty} \frac{k_1}{2\pi} = \lim_{\delta\to 0} \frac{k_1}{2\pi} = \frac{k_c\{\psi_{int}(z) = z\}}{2\pi} = \frac{k_{ES}}{2\pi} = 0.602\,677\,6(1). \tag{2.21}$$

2.2. *Wavenumbers of $O(\delta^{-1})$: the upper branch*

In order to carry through an analogous discussion also for the upper k-branch appearing in the bifurcation plot, we now consider values of k that vary proportionally to δ^{-1}, and rewrite the boundary value problem (2.1)–(2.8) by introducing the new rescaled quantities $\kappa \equiv 2\delta k$ and $\rho \equiv 2\delta R$, together with the rescaled independent variable

$$\xi \equiv z/(2\delta). \tag{2.22}$$

Then the rescaled wavenumber κ becomes independent of δ, i.e. $\kappa = O(\delta^0)$ and $\kappa^{-1} = O(\delta^0)$. Defining $\tilde{\boldsymbol{y}}(\xi) \equiv \boldsymbol{y}(z)$ and $\tilde{\phi}(\xi) \equiv \phi(z)$, the boundary value problem can be expressed in terms of the new quantities:

$$\tilde{y}_1' = 2\kappa\,[-\tilde{y}_1 + \tilde{y}_2], \tag{2.23}$$

$$\tilde{y}_2' = 2\kappa\left[\tfrac{1}{2}\tilde{y}_1 - \tilde{y}_2 + \tfrac{1}{2}\tilde{y}_4\right], \tag{2.24}$$

$$\tilde{y}_3' = -2\kappa\tilde{y}_3 - \frac{\rho}{\kappa}\,\tilde{\phi}'\tilde{y}_1, \tag{2.25}$$

$$\tilde{y}_4' = 2\kappa\,[-\tilde{y}_4 + \tilde{y}_5]\,, \tag{2.26}$$

$$\tilde{y}_5' = 2\kappa\left[\tfrac{1}{4}\tilde{y}_1 + \tfrac{1}{2}\tilde{y}_4 - \tilde{y}_5 + \tfrac{1}{4}\tilde{y}_6\right], \tag{2.27}$$

$$\tilde{y}_6' = 2\kappa\,[\tilde{y}_2 - \tilde{y}_6] + \frac{\rho}{2\kappa}\,\tilde{\phi}'\tilde{y}_3; \tag{2.28}$$

the initial condition is

$$\tilde{\boldsymbol{y}}(0) = (0,0,0,0,0,1)^T\,, \tag{2.29}$$

and the boundary condition reads

$$\tilde{y}_1\big(1/(2\delta)\big) = 0. \tag{2.30}$$

Note that the thickness of the boundary layers, originally characterized by δ, acquires the constant value $\frac{1}{2}$, so that now we have to distinguish the three regimes $0 \leqslant \xi \leqslant \frac{1}{2}$ (left-hand boundary layer), $\frac{1}{2} \leqslant \xi \leqslant 1/(2\delta) - \frac{1}{2}$ (interior) and $1/(2\delta) - \frac{1}{2} \leqslant \xi \leqslant 1/(2\delta)$ (right-hand boundary layer).

LEMMA 2.2. *Let $\psi(\xi)$ be some continuously differentiable function which is defined piecewise in the interval $\big[0, 1/(2\delta)\big]$ (with $0 < \delta < \frac{1}{2}$),*

$$\psi(\xi) = \begin{cases} \psi_{bl1}(\xi) & \text{for} \quad 0 \leqslant \xi \leqslant \frac{1}{2} \\ C & \text{for} \quad \frac{1}{2} < \xi < 1/(2\delta) - \frac{1}{2} \\ \psi_{bl2}(\xi) & \text{for} \quad 1/(2\delta) - \frac{1}{2} \leqslant \xi \leqslant 1/(2\delta), \end{cases} \tag{2.31}$$

where C is a constant, and let ρ_ψ be a positive constant. In addition, let $\tilde{\phi}_\delta(\xi)$ be a family of continuously differentiable functions defined in $\big[0, 1/(2\delta)\big]$, equipped with the following properties:

(i) *$\tilde{\phi}_\delta$ depends continuously on the parameter δ;*

(ii) *for each δ the shape of the boundary segments of the functions $\tilde{\phi}_\delta$ is determined by the boundary segments ψ_{bl1} and ψ_{bl2} of ψ,*

$$\tilde{\phi}_\delta'(\xi) = \begin{cases} \psi_{bl1}'(\xi) + O(\delta) & \text{for} \quad 0 \leqslant \xi \leqslant \frac{1}{2} \\ O\big(\delta^2\big) & \text{for} \quad \frac{1}{2} < \xi < 1/(2\delta) - \frac{1}{2} \\ \psi_{bl2}'(\xi) + O(\delta) & \text{for} \quad 1/(2\delta) - \frac{1}{2} \leqslant \xi \leqslant 1/(2\delta). \end{cases} \tag{2.32}$$

Then it follows that each component of the solution vector $\tilde{\boldsymbol{y}}_\psi$ originating from the initial value problem (2.23)–(2.29) with input quantities κ, $\rho = \rho_\psi$, and $\tilde{\phi}(\xi) = \psi(\xi)$ differs from the corresponding component of the solution vector $\tilde{\boldsymbol{y}}_\delta$ resulting from the input κ, ρ_ψ, and $\tilde{\phi}(\xi) = \tilde{\phi}_\delta(\xi)$ in the entire interval $\big[0, 1/(2\delta)\big]$ at most by an amount of $O(\delta)$,

$$\tilde{\boldsymbol{y}}_\delta(\xi) = \tilde{\boldsymbol{y}}_\psi(\xi) + O(\delta)\,. \tag{2.33}$$

Proof. Within the boundary layers $0 \leqslant \xi \leqslant \frac{1}{2}$ and $1/(2\delta) - \frac{1}{2} \leqslant \xi \leqslant 1/(2\delta)$ we can carry through the proof in a manner analogous to the proof of lemma 2.1. But in the interior regime $\frac{1}{2} \leqslant \xi \leqslant 1/(2\delta) - \frac{1}{2}$ this line of reasoning does not work (Nicodemus 1997). We thus need a sharper argument: introducing an auxiliary perturbation parameter ϵ, we write

$$\tilde{\boldsymbol{y}}_\delta'(\xi) = \left[2\kappa\boldsymbol{A}_0 + \epsilon\,\frac{\rho_\psi}{\kappa}\,\tilde{\phi}_\delta'(\xi)\,\boldsymbol{A}_1\right]\tilde{\boldsymbol{y}}_\delta(\xi) \quad \text{for} \quad \tfrac{1}{2} \leqslant \xi \leqslant 1/(2\delta) - \tfrac{1}{2}$$

with initial condition (2.33) at $\xi = \frac{1}{2}$, where $\boldsymbol{A}_0$ and $\boldsymbol{A}_1$ are matrices with constant coefficients defined by

$$\boldsymbol{A}_0 \equiv \begin{pmatrix} -1 & 1 & 0 & 0 & 0 & 0 \\ \frac{1}{2} & -1 & 0 & \frac{1}{2} & 0 & 0 \\ 0 & 0 & -1 & 0 & 0 & 0 \\ 0 & 0 & 0 & -1 & 1 & 0 \\ \frac{1}{4} & 0 & 0 & \frac{1}{2} & -1 & \frac{1}{4} \\ 0 & 1 & 0 & 0 & 0 & -1 \end{pmatrix}, \quad \boldsymbol{A}_1 \equiv \begin{pmatrix} 0 & 0 & 0 & 0 & 0 & 0 \\ 0 & 0 & 0 & 0 & 0 & 0 \\ -1 & 0 & 0 & 0 & 0 & 0 \\ 0 & 0 & 0 & 0 & 0 & 0 \\ 0 & 0 & 0 & 0 & 0 & 0 \\ 0 & 0 & \frac{1}{2} & 0 & 0 & 0 \end{pmatrix}. \tag{2.34}$$

For $\epsilon = 1$ this initial value problem is the one to be studied. Using the ansatz

$$\widetilde{\boldsymbol{y}}_\delta(\xi) = \sum_{n=0}^{\infty} \epsilon^n \widetilde{\boldsymbol{y}}_{\delta,n}(\xi)\,; \quad \widetilde{\boldsymbol{y}}_{\delta,0}\left(\tfrac{1}{2}\right) = \widetilde{\boldsymbol{y}}_\delta\left(\tfrac{1}{2}\right), \quad \widetilde{\boldsymbol{y}}_{\delta,n}\left(\tfrac{1}{2}\right) = 0 \quad \text{for} \quad n \geqslant 1,$$

we solve this problem order by order in the perturbation parameter ϵ. $O\left(\epsilon^0\right)$ produces the problem

$$\widetilde{\boldsymbol{y}}'_{\delta,0}(\xi) = 2\kappa \boldsymbol{A}_0 \widetilde{\boldsymbol{y}}_{\delta,0}(\xi), \quad \widetilde{\boldsymbol{y}}_{\delta,0}\left(\tfrac{1}{2}\right) = \widetilde{\boldsymbol{y}}_\delta\left(\tfrac{1}{2}\right),$$

the solution of which is given by

$$\begin{aligned} \widetilde{\boldsymbol{y}}_{\delta,0}(\xi) &= \mathrm{e}^{2\kappa \boldsymbol{A}_0\left(\xi - 1/2\right)} \widetilde{\boldsymbol{y}}_\delta\left(\tfrac{1}{2}\right) = \mathrm{e}^{2\kappa \boldsymbol{A}_0\left(\xi - 1/2\right)} \left[\widetilde{\boldsymbol{y}}_\psi\left(\tfrac{1}{2}\right) + O(\delta)\right] \\ &= \widetilde{\boldsymbol{y}}_\psi(\xi) + \mathrm{e}^{2\kappa \boldsymbol{A}_0\left(\xi - 1/2\right)} \times O(\delta). \end{aligned}$$

Because the largest eigenvalue of $\boldsymbol{A}_0$ is zero, cf. the Appendix, we have for $\xi \geqslant \frac{1}{2}$

$$\mathrm{e}^{2\kappa \boldsymbol{A}_0\left(\xi - 1/2\right)} = O\left(\delta^0\right),$$

and we find

$$\widetilde{\boldsymbol{y}}_{\delta,0}(\xi) = \widetilde{\boldsymbol{y}}_\psi(\xi) + O(\delta) \quad \text{for} \quad \tfrac{1}{2} \leqslant \xi \leqslant 1/(2\delta) - \tfrac{1}{2}. \tag{2.35}$$

For $n \geqslant 1$ the ϵ-expansion yields

$$\widetilde{\boldsymbol{y}}'_{\delta,n}(\xi) = 2\kappa \boldsymbol{A}_0 \widetilde{\boldsymbol{y}}_{\delta,n}(\xi) + \frac{\rho_\psi}{\kappa} \tilde{\phi}'_\delta(\xi)\, \boldsymbol{A}_1 \widetilde{\boldsymbol{y}}_{\delta,n-1}(\xi), \quad \widetilde{\boldsymbol{y}}_{\delta,n}\left(\tfrac{1}{2}\right) = 0.$$

With the help of the solution

$$\widetilde{\boldsymbol{y}}_{\delta,n}(\xi) = \frac{\rho_\psi}{\kappa} \int_{1/2}^{\xi} \mathrm{d}t\, \mathrm{e}^{2\kappa \boldsymbol{A}_0(\xi - t)}\, \tilde{\phi}'_\delta(t)\, \boldsymbol{A}_1 \widetilde{\boldsymbol{y}}_{\delta,n-1}(t)$$

we conclude via complete induction

$$\widetilde{\boldsymbol{y}}_{\delta,n}(\xi) = O(\delta^n) \quad \text{for} \quad \tfrac{1}{2} \leqslant \xi \leqslant 1/(2\delta) - \tfrac{1}{2}. \tag{2.36}$$

Thus, for $\epsilon = 1$ one obtains from (2.35) and (2.36)

$$\widetilde{\boldsymbol{y}}_\delta(\xi) = \widetilde{\boldsymbol{y}}_\psi(\xi) + O(\delta) + \sum_{n=1}^{\infty} O(\delta^n) = \widetilde{\boldsymbol{y}}_\psi(\xi) + O(\delta) \quad \text{for} \quad \tfrac{1}{2} \leqslant \xi \leqslant 1/(2\delta) - \tfrac{1}{2}.$$

□

In order to exploit this lemma 2.2 for the high-*Re* analysis of the eigenvalue problem (2.1)–(2.8), we now introduce the *shape functions for the boundary layers* $\psi_{bl}(\xi)$ as continuously differentiable functions defined in the interval $[0, 1]$ that satisfy the boundary and symmetry conditions

$$\psi_{bl}(0) = 0, \quad \psi_{bl}(1) = 1, \quad \text{and} \quad \psi_{bl}(\xi) = 1 - \psi_{bl}(1 - \xi), \tag{2.37}$$

and have vanishing slope at $\xi = \frac{1}{2}$,

$$\psi'_{bl}\left(\tfrac{1}{2}\right) = 0. \tag{2.38}$$

In addition, we consider for each given ψ_{bl} the function

$$\psi(\xi) \equiv \begin{cases} \psi_{bl}(\xi) & \text{for} \quad 0 \leqslant \xi \leqslant \frac{1}{2} \\ \frac{1}{2} & \text{for} \quad \frac{1}{2} < \xi < 1/(2\delta) - \frac{1}{2} \\ \psi_{bl}\left(\xi - \left(1/(2\delta) - 1\right)\right) & \text{for} \quad 1/(2\delta) - \frac{1}{2} \leqslant \xi \leqslant 1/(2\delta). \end{cases} \tag{2.39}$$

This ψ is a (symmetric) example of the function appearing in lemma 2.2, see (2.31). If one cuts out the interior part where ψ is constant and connects the two remaining boundary segments, one recovers the shape functions ψ_{bl}. Note that these shape functions do not depend on the parameter δ, just as the previous shape functions ψ_{int} do not depend on the parameter p_δ.

As in the application of lemma 2.1, we consider families of functions $\phi_\delta(z)$ which satisfy (2.16), so that each ϕ_δ is a candidate profile for the variational principle, but now each member of the family inherits its shape within the boundary layers from ψ_{bl}:

$$\phi'_\delta(z) = \begin{cases} \psi'_{bl}\left(z/(2\delta)\right)/(2\delta) + O\left(\delta^0\right) & \text{for} \quad 0 \leqslant z \leqslant \delta \\ O(\delta) & \text{for} \quad \delta < z \leqslant \frac{1}{2}. \end{cases} \tag{2.40}$$

For preassigned rescaled wavenumber κ, we set for each δ the parameter ρ_ψ required in lemma 2.2 to the smallest positive ρ-value for which the boundary value problem (2.23)–(2.30) with $\tilde{\phi}(\xi) = \psi(\xi)$ as input can be solved. We denote this value as $\rho_0\{\psi\}(\kappa)$. Then (2.33) yields the assertion

$$\lim_{\delta \to 0} 2\delta \, R_0\{\phi_\delta\}\left(\kappa/(2\delta)\right) = \lim_{\delta \to 0} \rho_0\{\psi\}(\kappa), \tag{2.41}$$

so that we can relate the critical rescaled Reynolds numbers pertaining to the actual profiles to a functional which contains information about the profiles in the boundary layers only. Comparing (2.41) to (2.17), a major technical difference between these two equations becomes obvious: both sides of (2.41) explicitly require that a limit $\delta \to 0$ be taken. As shown in the Appendix, the right-hand side of (2.41) can be evaluated by recasting the boundary value problem (2.23)–(2.30) for input profiles ψ into a simpler boundary value problem which refers only to the right-hand boundary segment of the shape function ψ_{bl}.

This reduced boundary value problem consists of the system (2.23)–(2.28), considered in the interval $\left[\frac{1}{2}, 1\right]$, with initial condition

$$\tilde{\boldsymbol{y}}\left(\tfrac{1}{2}\right) = (1, 1, 0, 1, 1, 1)^T \tag{2.42}$$

and boundary condition

$$\tilde{y}_1(1) = 0. \tag{2.43}$$

Denoting the smallest positive ρ-value for which this boundary value problem is solved with κ and ψ_{bl} as input as $\sigma_0\{\psi_{bl}\}(\kappa)$, the main result obtained in the Appendix, see (A 18), can be expressed in the form

$$\lim_{\delta \to 0} \rho_0\{\psi\}(\kappa) = \sigma_0\{\psi_{bl}\}(\kappa).$$

The possibility of reducing the boundary value problem in this manner hinges on the following: if we have a function ψ which is constant in the interior as an input for the system (2.23)–(2.28), then these equations can be integrated analytically in the

interior. If one approaches the limit $\delta \to 0$, the interior range becomes so long that it is only the eigenvector corresponding to the largest (non-degenerate) eigenvalue of the coefficient matrix that determines the solution at the connection point to the right-hand boundary layer. Consequently, the initial conditions (2.42) have been chosen proportional to this eigenvector. The original system of differential equations (I, 3.22)–(I, 3.27) derived directly from the restricted Couette problem had been transformed in §4 of Part 1 with a common exponential factor e^{-2kz}, resulting in the system (2.1)–(2.6) considered here. The guiding principle behind this transformation was to ensure that the largest eigenvalue of the coefficient matrix that emerges when the profile function is replaced by a constant is equal to zero. Each damping constant not equal to $2k$ would have produced a non-vanishing largest eigenvalue and, in turn, would have made the numerical analysis for high Reynolds numbers exceedingly difficult, if not impossible.

Our assertion (2.41) therefore now becomes a statement for $R_0\{\phi_\delta\}$ that acquires the form of (2.17),

$$\lim_{\delta\to 0} 2\delta\, R_0\{\phi_\delta\}\big(\kappa/(2\delta)\big) = \sigma_0\{\psi_{bl}\}(\kappa), \tag{2.44}$$

and we can proceed in close analogy to the previous case. When considering $\sigma_0\{\psi_{bl}\}(\kappa)$ as a function of the rescaled wavenumber κ, we know that this function must have a global minimum for some $\kappa > 0$; the minimizing κ is manifestly independent of δ and therefore of the required order, $O\big(\delta^0\big)$. For sufficiently small δ, (2.44) relates this minimum to the minima corresponding to the actual profiles. Hence, for profile families ϕ_δ that merely satisfy (2.16) and (2.40) we have obtained a further far-reaching statement: *for small δ, and provided k is of $O\big(\delta^{-1}\big)$, we can understand the k-dependencies of $R_0\{\phi_\delta\}(k)$ as being mirror images of the k-dependence of $\sigma_0\{\psi_{bl}\}(\kappa)$, where $\kappa = 2\delta k$, and the function ψ_{bl} contains the information about the profiles ϕ_δ in the boundary layers.*

Focusing on the minima of $R_0\{\phi_\delta\}\big(\kappa/(2\delta)\big)$, the conclusion that parallels (2.19) reads

$$\lim_{\delta\to 0} 2\delta R_2\{\phi_\delta\} = \sigma_c\{\psi_{bl}\}, \tag{2.45}$$

where

$$R_2\{\phi_\delta\} \equiv \min_{k=O\left(\delta^{-1}\right)} \{R_0\{\phi_\delta\}(k)\} \tag{2.46}$$

and $\sigma_c\{\psi_{bl}\} \equiv \min_{\kappa>0} \{\sigma_0\{\psi_{bl}\}(\kappa)\}$; the minimizing κ will be written as $\kappa_c\{\psi_{bl}\}$.

The fruits of these efforts now consist in a first understanding of the upper k-branch appearing in the bifurcation plot, referred to as k_2, if we take again the scaling properties (I, 5.4) for granted. With

$$\psi_{bl}(\xi) = \begin{cases} 2\xi\,(1-\xi) & \text{for} \quad 0 \leqslant \xi \leqslant \frac{1}{2} \\ 1 - 2\xi\,(1-\xi) & \text{for} \quad \frac{1}{2} < \xi \leqslant 1 \end{cases} \tag{2.47}$$

as boundary layer shape function for the profiles (I, 4.1), we obtain for $0 \leqslant z \leqslant \delta$

$$\phi'_\delta(z) = \frac{\psi'_{bl}\big(z/(2\delta)\big)}{2\delta} + O\big(\delta^0\big),$$

whereas for $\delta < z \leqslant \frac{1}{2}$ we have $\phi'_\delta(z) = O(\delta)$. Thus, the condition (2.40) required to deduce (2.45) is satisfied, and we obtain a minimizing k-branch with the asymptotic behaviour

$$\lim_{\delta\to 0} 2\delta\, \frac{k}{2\pi} = \frac{\kappa_c\{\psi_{bl}\}}{2\pi}. \tag{2.48}$$

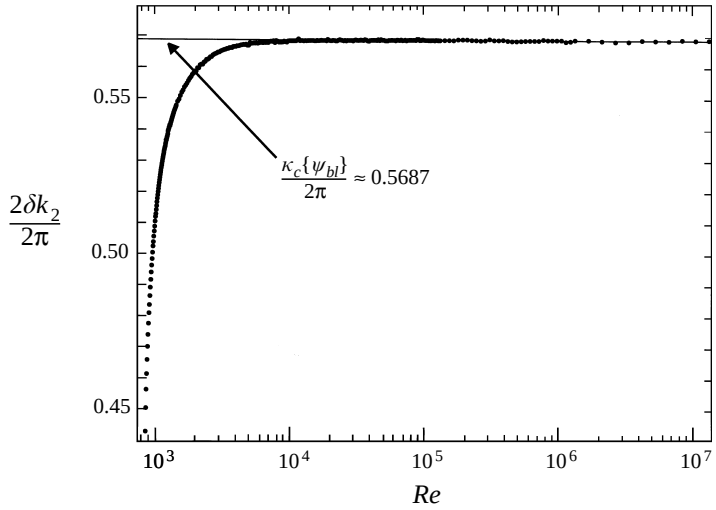

FIGURE 1. Comparison of $2\delta k_2/2\pi$, calculated numerically for the profile class (I, 4.1) as described in § 5 of Part 1 (points), to the constant (2.50) (solid line, indicated by the arrow).

Numerical computations performed with the boundary layer shape function (2.47) yield the values

$$\sigma_c\{\psi_{bl}\} = 400.469\,295\,814\,41(1), \tag{2.49}$$

$$\frac{\kappa_c\{\psi_{bl}\}}{2\pi} = 0.568\,719\,56(2). \tag{2.50}$$

In figure 1 we compare $2\delta k_2/2\pi$, calculated as a function of the Reynolds number Re from the numerical data reported in § 5 of Part 1, to the constant value (2.50).

3. Scaling solutions to the variational principle

In the previous section we have studied the equations which embody the spectral constraint (I, 2.13) and understood the main consequence that this constraint has for the functions $R_0\{\phi\}(k)$: if the profiles $\phi(z)$ are characterized by two shape functions $\psi_{int}(z)$ and $\psi_{bl}(\xi)$, and if the Reynolds numbers become large, then $R_0\{\phi\}(k)$ exhibits (at least) two distinct minima. But we do not yet understand two further key observations made in the numerical analysis: first, the optimal upper bound on the energy dissipation rate is not determined by an individual minimum, but after optimization both R_0, (2.18) and (2.46), turn out to be equal. Second, the numerically found optimal profile parameters δ and p exhibit a pronounced scaling behaviour with Re. In order to explain these findings, we now have to analyse the variational principle itself.

Given a shape function $\psi_{int}(z)$ with the properties (2.14) and (2.15), and a shape function $\psi_{bl}(\xi)$ with properties (2.37) and (2.38), we now specify a profile family whose members $\phi_{\delta,p}(z)$ are continuously differentiable with respect to z, and depend continuously on the parameters δ and p, by two requirements:

(i) each $\phi_{\delta,p}$ obeys the boundary conditions and the symmetry condition (2.16), so that each $\phi_{\delta,p}$ is a candidate profile for the variational principle;

(ii) for each δ and p the derivative of $\phi_{\delta,p}$ be determined by the derivatives of the

shape functions ψ_{int} and ψ_{bl} according to

$$\phi'_{\delta,p}(z) = \begin{cases} \psi'_{bl}\big(z/(2\delta)\big)/(2\delta) + p \times O\big(\delta^{-1}\big) & \text{for} \quad 0 \leqslant z \leqslant \delta \\ p\,\psi'_{int}(z) & \text{for} \quad \delta < z < 1-\delta \\ \psi'_{bl}\big(1-(1-z)/(2\delta)\big)/(2\delta) + p \times O\big(\delta^{-1}\big) & \text{for} \quad 1-\delta \leqslant z \leqslant 1. \end{cases} \tag{3.1}$$

In contrast to the previous section, δ and p are now regarded as independent parameters; the values of p range from zero to an upper bound that may depend on δ.

It can easily be verified that the profiles (I, 4.1) constitute such a family: the corresponding shape functions are given by (2.20) and (2.47). It needs to be stressed that the above specification of the profile family does, by itself, not imply any type of relation between the parameters δ and p. The profiles $\phi_{\delta,p}$ have been chosen such that the lemmas 2.1 and 2.2 can be applied, provided the propositions (2.12) and (2.40) can be fulfilled, which is not guaranteed by the above two requirements (i) and (ii).

We will now determine, within this profile family $\phi_{\delta,p}$, the optimal upper bound on c_ε for given asymptotically large rescaled Reynolds number R. In that case the profile functional (I, 2.11)

$$D\{\phi_{\delta,p}\} = \int_0^1 \mathrm{d}z\, \big[\phi'_{\delta,p}(z)\big]^2 - 1 \tag{3.2}$$

takes on large values, as a consequence of the spectral constraint (I, 2.13). Hence, when seeking solutions to the variational principle (I, 2.12) with this constraint, we can expand both the required root of the cubic polynomial (I, 2.20) that yields the corresponding Reynolds number via (I, 2.19), and the right-hand side of (I, 2.12), in powers of $D\{\phi_{\delta,p}\}^{-1}$:

$$Re = \tfrac{2}{3} R[1 + \tfrac{4}{27} D\{\phi_{\delta,p}\}^{-1} + O(D\{\phi_{\delta,p}\}^{-2})], \tag{3.3}$$

$$\overline{c_\varepsilon} = \frac{27}{16} \frac{D\{\phi_{\delta,p}\}}{R} [1 + \tfrac{8}{9} D\{\phi_{\delta,p}\}^{-1} + O(D\{\phi_{\delta,p}\}^{-2})], \tag{3.4}$$

where $\overline{c_\varepsilon}$ denotes the upper bound on c_ε given by the expression in curly brackets on the right-hand side of (I, 2.12). We conclude: if, for sufficiently large R, the profile function $\phi_{\delta,p}$ that minimizes the profile functional (3.2) has been found, then this same function yields the lowest possible upper bound on the energy dissipation rate at a Reynolds number slightly above the asymptotic value $\frac{2}{3}R$. Whereas $D\{\phi_{\delta,p}\}$ gives only a small correction to $Re = \frac{2}{3}R$, the leading term of the expansion of $\overline{c_\varepsilon}$ is directly proportional to $D\{\phi_{\delta,p}\}$. Thus, if R is asymptotically large, minimizing the upper bound $\overline{c_\varepsilon}$ is tantamount to minimizing the profile functional $D\{\phi_{\delta,p}\}$ under the spectral constraint.

The profile functional (3.2) measures the deviation of its argument from the laminar profile; it takes on values ranging from zero (for the laminar profile) to infinity. We now demand that the deviation of our variational profiles $\phi_{\delta,p}$ from the laminar profile, as measured by $D\{\phi_{\delta,p}\}$, be monotonic in both δ and p. That is, in addition to the properties (i) and (ii) listed above, we specify the family $\phi_{\delta,p}$ by a third requirement:

(iii) the dependence of the profiles on δ and p be such that

$$\frac{\partial D\{\phi_{\delta,p}\}}{\partial p} < 0 \quad \text{(for fixed } \delta\text{)} \quad \text{and} \quad \frac{\partial D\{\phi_{\delta,p}\}}{\partial \delta} < 0 \quad \text{(for fixed } p\text{)}. \tag{3.5}$$

This third specification, which restricts the possible functions ψ_{int} and ψ_{bl}, makes sure that the measure for the deviation from the laminar profile increases if the slope p or the extension of the boundary layer decreases. The previous family (I, 4.1) obviously obeys these monotonic conditions, see (I, 4.2).

Since we already know that minimizing the upper bound on c_ε for a given large R means minimizing $D\{\phi_{\delta,p}\}$, the requirements (3.5) imply that the minimal upper bound is attained if both parameters δ and p take on, independently from each other, the largest values that are permitted by the spectral constraint. We denote these values as δ_R and p_R. Now we can utilize the relations (2.19) and (2.45). It must be kept in mind, however, that these relations hold only if the conditions (2.12) and (2.40) are satisfied. We will therefore first assume that this is the case, and deduce the ensuing scaling properties of δ_R and p_R. In a second step we will show that these scaling properties actually suffice to guarantee that the conditions are fulfilled, so that the argument is self-consistent. This indirect strategy is the price to pay for the detailed statements that we will obtain about the highly nonlinear variational principle.

Assuming that the conditions are satisfied, then (2.19) and (2.45) hold. Since the variational principle forces δ and p to their largest possible values δ_R and p_R, respectively, $R_1\{\phi_{\delta,p}\}$ and $R_2\{\phi_{\delta,p}\}$ take on, independently from each other, the smallest possible values compatible with the spectral constraint. By the very definition of the spectral constraint, the infimum of both $R_1\{\phi_{\delta,p}\}$ and $R_2\{\phi_{\delta,p}\}$ is R itself:

$$R_1\{\phi_{\delta_R,p_R}\} = R_2\{\phi_{\delta_R,p_R}\} = R. \tag{3.6}$$

This is the mechanism that locks the two minima to the same value. Hence, we obtain from (2.19) and (2.45) the asymptotic behaviour of the optimal parameters δ_R and p_R:

$$\delta_R \sim \frac{\sigma_c\{\psi_{bl}\}}{2R}, \quad p_R \sim \frac{R_c\{\psi_{int}\}}{R}. \tag{3.7}$$

To check the consistency of this reasoning we have to insert (3.7) into (3.1). Since

$$p_R \sim \frac{2R_c\{\psi_{int}\}}{\sigma_c\{\psi_{bl}\}}\,\delta_R,$$

i.e. $p_R = O(\delta_R)$, we find for $0 \leqslant z \leqslant \delta_R$ the estimate

$$\phi'_{\delta_R,p_R}(z) = \frac{\psi'_{bl}\big(z/(2\delta_R)\big)}{2\delta_R} + p_R \times O\big(\delta_R^{-1}\big) = \frac{\psi'_{bl}\big(z/(2\delta_R)\big)}{2\delta_R} + O\big(\delta_R^{0}\big) = O\big(\delta_R^{-1}\big)\,;$$

analogously, $\phi'_{\delta_R,p_R}(z) = O\big(\delta_R^{-1}\big)$ for $1-\delta_R \leqslant z \leqslant 1$. On the other hand, for $\delta_R < z < 1-\delta_R$ we have $\phi'_{\delta_R,p_R}(z) = O(\delta_R)$. Thus, the conditions (2.12) and (2.40) required to guarantee the validity of (2.19) and (2.45) are satisfied.

From now on we write δ and p for the optimized parameters, omitting the subscript R. By virtue of (3.3) the limit $R \to \infty$ is equivalent to the limit $Re \to \infty$. Hence, *we have proven a generalization of the numerically found scaling law (I, 5.4):*

$$\delta \sim \alpha Re^{-1}, \quad p \sim \beta Re^{-1};$$

the scaling constants are identified as $\alpha = \frac{1}{3}\sigma_c\{\psi_{bl}\}$ and $\beta = \frac{2}{3}R_c\{\psi_{int}\}$. This type of scaling holds for all profile families that stem from two shape functions and obey the specifications (i), (ii), and (iii). It has to be emphasized that the practical calculation of $R_c\{\psi_{int}\}$ and $\sigma_c\{\psi_{bl}\}$ from their respective eigenvalue problems, followed by a

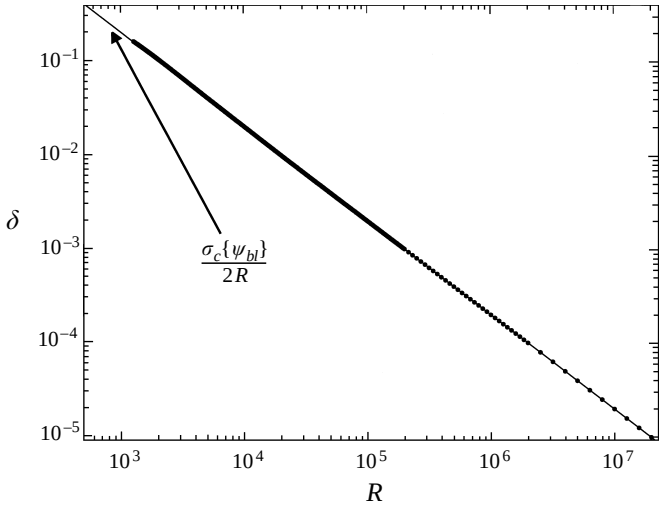

FIGURE 2. Comparison of the optimized parameter δ, as obtained in the numerical solution of the variational principle with the profile family (I, 4.1) for $Re \geqslant Re_B$ (points; cf. Part 1, figure 5), to the scaling solution (3.7) (solid line, indicated by the arrow).

minimization over the (rescaled) wavenumber, is much simpler than solving the full problem for the corresponding high-R profiles.

To demonstrate the accuracy of our arguments, we resort once again to the profile family (I, 4.1) and compare the analytically derived scaling behaviour (3.7) to the corresponding data obtained in the numerical solution of the variational problem. With $R_c\{\psi_{int}(z) = z\} = Re_{ES}$, see (I, 5.1), and $\sigma_c\{\psi_{bl}\}$ from (2.49) we obtain δ and p as functions of R. In figures 2 and 3 we show that there is excellent agreement between the numerical data and the asymptotic laws for $R > 2000$. We then can utilize these power laws to derive asymptotic expressions for the optimized profile functional $D\{\phi_{\delta,p}\}$, the Reynolds number Re, and the optimal bound $\overline{c_\varepsilon}$ as functions of R, see (3.2)–(3.4). In figure 4 we depict this asymptotic bound as a function of Re in comparison with the numerical data, taken from figure 3 of Part 1. Most remarkably, the asymptotic bound captures even the ascent of the numerical data from the minimum point to the high-Re limit.

4. The limit $Re = \infty$: variational principle for the asymptotic boundary layer shape function

In this section we try to obtain the best bound on the energy dissipation rate that the variational principle can provide for infinitely large Reynolds numbers. We start from a profile family $\phi_{\delta,p}(z)$ that obeys the specifications (i), (ii), and (iii) formulated in the previous section. Applied to this family, the variational principle (I, 2.12), (I, 2.13) yields the scaling solutions (3.7) for the parameters δ and p. Since now we are only interested in the asymptotic value $\lim_{Re\to\infty} \overline{c_\varepsilon}(Re) \equiv \overline{c_\varepsilon^\infty}$ of the upper bound, we conclude from § 2.2 that we may take the limit $p \overset{Re\to\infty}{\longrightarrow} 0$ first, and then $\delta \overset{Re\to\infty}{\longrightarrow} 0$. That is, we will obtain the correct value of $\overline{c_\varepsilon^\infty}$ if we set $p = 0$ right from the outset, and then take the limit $\delta \to 0$.

Inserting $p = 0$ into (3.1) and utilizing (2.37) and (2.16), we arrive at the one-

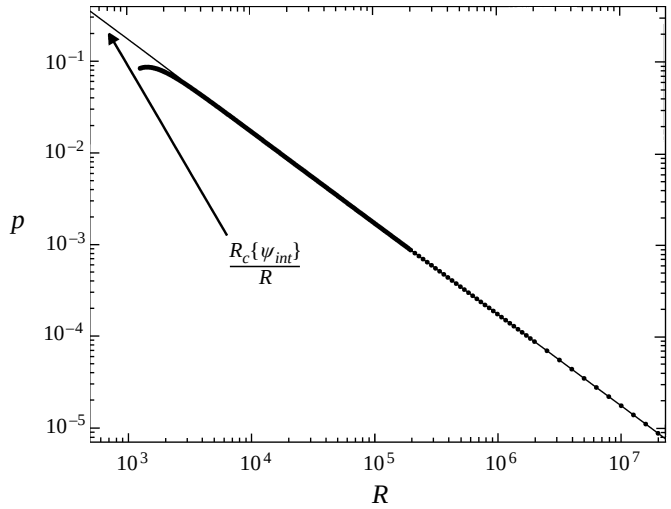

FIGURE 3. Comparison of the optimized parameter p, as obtained in the numerical solution of the variational principle with the profile family (I, 4.1) for $Re \geqslant Re_B$ (points; cf. Part 1, figure 6), to the scaling solution (3.7) (solid line, indicated by the arrow).

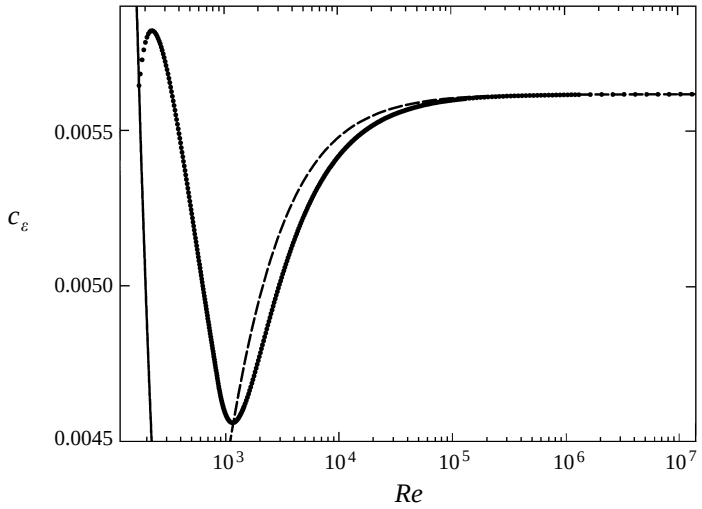

FIGURE 4. Comparison of the asymptotic upper bound on c_ε, as obtained numerically with the profile family (I, 4.1) (points, cf. Part 1, figure 3), to the asymptotic bound resulting from the scaling solution (3.7) (long-dashed line). The solid line at the left shows the lower bound $\underline{c_\varepsilon}(Re) = Re^{-1}$.

parameter profile family

$$\phi_{\delta,0}(z) = \begin{cases} \psi_{bl}\big(z/(2\delta)\big) & \text{for} \quad 0 \leqslant z \leqslant \delta \\ \frac{1}{2} & \text{for} \quad \delta < z < 1-\delta \\ \psi_{bl}\big(1-(1-z)/(2\delta)\big) & \text{for} \quad 1-\delta \leqslant z \leqslant 1. \end{cases} \tag{4.1}$$

With $\xi = z/(2\delta)$, as in (2.22), the right-hand side of (4.1) equals the function $\psi(\xi)$ defined in (2.39). In order to compute $\overline{c_\varepsilon^\infty}$, we first evaluate the profile functional

$D\{\phi_{\delta,0}\}$. Since we have $\delta = \sigma_c\{\psi_{bl}\}/(2R)$ from (3.7), we find

$$D\{\phi_{\delta,0}\} = \frac{R}{\sigma_c\{\psi_{bl}\}} \int_0^1 \mathrm{d}\xi \left[\psi'_{bl}(\xi)\right]^2 - 1. \tag{4.2}$$

Then (3.3) and (3.4) yield

$$\overline{c_\varepsilon^\infty} = \frac{27}{16} \frac{I\{\psi_{bl}\}}{\sigma_c\{\psi_{bl}\}}, \tag{4.3}$$

where we have introduced the new functional

$$I\{\psi_{bl}\} \equiv \int_0^1 \mathrm{d}\xi \left[\psi'_{bl}(\xi)\right]^2. \tag{4.4}$$

Clearly, the asymptotic bound $\overline{c_\varepsilon^\infty}$ depends on the shape of the boundary layers only, as determined by the shape function ψ_{bl}.

In this way we have obtained a rigorous asymptotic upper bound on c_ε for each ψ_{bl} that is of the required form. Hence, the best possible asymptotic upper bound within all families $\phi_{\delta,p}$ is determined by a new variational principle:

$$\lim_{Re\to\infty} c_\epsilon(Re) \leqslant \inf_{\psi_{bl}} \left\{ \frac{27}{16} \frac{I\{\psi_{bl}\}}{\sigma_c\{\psi_{bl}\}} \right\}, \tag{4.5}$$

where ψ_{bl} is an arbitrary continuously differentiable function defined on the interval $[0, 1]$ with the properties (2.37) and (2.38), the functional $I\{\psi_{bl}\}$ is given by (4.4), and $\sigma_c\{\psi_{bl}\} = \min_{\kappa>0}\{\sigma_0\{\psi_{bl}\}(\kappa)\}$; the eigenvalue $\sigma_0\{\psi_{bl}\}(\kappa)$ has to be determined as the smallest positive ρ-value solving the boundary value problem (2.23)–(2.28), (2.42) and (2.43) with κ and ψ_{bl} as input.

The key point is that this new principle (4.5) is much simpler than the original principle (I, 2.12), (I, 2.13), evaluated at asymptotically high *Re*. The new principle can therefore be solved employing profiles with rather complicated boundary segments (described by the boundary layer shape functions ψ_{bl}), even non-analytical ones, which is practically impossible on the level of the original principle. By such an extensive numerical investigation of (4.5), we found that at least a rather good approximation to this principle's solution can be obtained within the following one-parameter class of shape functions:

$$\psi_{bl}^{(n)}(\xi) \equiv \begin{cases} \frac{1}{2} - 2^{n-1}\left(\frac{1}{2} - \xi\right)^n & \text{for} \quad 0 \leqslant \xi \leqslant \frac{1}{2} \\ \frac{1}{2} + 2^{n-1}\left(\xi - \frac{1}{2}\right)^n & \text{for} \quad \frac{1}{2} < \xi \leqslant 1 \end{cases}, \quad n \geqslant 2. \tag{4.6}$$

For each function $\psi_{bl}^{(n)}$, the boundary segments (i.e. the parts of $\psi_{bl}^{(n)}$ defined in $0 \leqslant \xi \leqslant \frac{1}{2}$ and $\frac{1}{2} < \xi \leqslant 1$, respectively) are modelled by polynomials of order n which have the property that the first $n-1$ derivatives vanish at the matching point $\xi = \frac{1}{2}$. For $n = 2$, in particular, the function $\psi_{bl}^{(2)}$ is identical with the boundary layer shape function (2.47) for the profile family (I, 4.1).

Unexpectedly, the best possible asymptotic upper bound on c_ε within the class (4.6) is given by the limiting shape function $\lim_{n\to\infty} \psi_{bl}^{(n)}(\xi)$. With increasing n the functions $\psi_{bl}^{(n)}$ develop distinct internal boundary layers within the previous boundary layers. The widths of these new internal layers can be characterized by the shape functions' inverse slopes at the origin $\xi = 0$, namely $\left[\psi_{bl}^{(n)\prime}(0)\right]^{-1} = 1/n$. It needs to be emphasized that it is, nonetheless, the shape of the functions $\psi_{bl}^{(n)}$ in the entire intervals $0 \leqslant \xi \leqslant \frac{1}{2}$ and $\frac{1}{2} < \xi \leqslant 1$ that determines the bound on c_ε. If one replaced,

n	$\sigma_c\{\psi_{bl}^{(n)}\}$	$\overline{c_\epsilon^\infty}^{(n)}$
2	400.46929581441(1)	$0.561840826129 83(1) \times 10^{-2}$
3	570.26826714776(1)	$0.532644051052 02(1) \times 10^{-2}$
4	740.09950462354(2)	$0.521165442355 60(2) \times 10^{-2}$
10	1757.8719829105(2)	$0.505246060789 0(1) \times 10^{-2}$
100	17007.03473085(3)	$0.49861128831 0(1) \times 10^{-2}$
1000	169488.035203(1)	$0.49807178721 1(2) \times 10^{-2}$
10000	1694296.84184(2)	$0.49801910076 9(6) \times 10^{-2}$
100000	16942384.78(1)	$0.49801384 50(3) \times 10^{-2}$
1000000	169423262(2)	$0.49801332 6(6) \times 10^{-2}$

TABLE 1. Asymptotic upper bounds on c_ε provided by shape functions (4.6) for increasing values of n.

for some large n, the internal boundary layers of thickness $1/n$ by the corresponding segments from $\psi_{bl}^{(2)}$, shortened to $1/n$, and then linked these two quadratic segments with a constant piece $\psi(\xi) = \frac{1}{2}$ for $1/n < \xi < 1 - 1/n$, one would merely obtain the same value for the upper bound as $\psi_{bl}^{(2)}$ would have produced itself, not the better bound resulting from $\psi_{bl}^{(n)}$.

In table 1 we present the numerical values for $\sigma_c\left\{\psi_{bl}^{(n)}\right\}$ and the resulting asymptotic upper bounds on c_ε, denoted as $\overline{c_\epsilon^\infty}^{(n)}$, for increasing values of n. In particular, $\overline{c_\epsilon^\infty}^{(2)}$ equals the previously obtained bound (I, 5.3). Obviously, the data allow us to extract the limit $n \to \infty$ with considerable accuracy:

$$\lim_{n\to\infty} \overline{c_\epsilon^\infty}^{(n)} = 0.498\,013\,3(1) \times 10^{-2}. \tag{4.7}$$

Thus, the improvement that results from the optimization of the shape of the boundary segments amounts to about 11%.

5. Incorporating a variational parameter for the shape of the boundary segments

We now come back to the variational principle (I, 2.12), (I, 2.13) and to the solution technique developed in §§ 3 and 4 of Part 1. The previous test profiles (I, 4.1), chosen on the grounds of a simple guess, had been characterized merely by the thickness δ of the profiles' boundary segments and by their slope p in the interior. However, the analysis carried through in the preceding section has revealed that in order to find the best high-Re bound on c_ε that is obtainable from the background flow method one has to resort to test profiles $\phi(z)$ that contain at least one variational parameter governing the shape of the boundary segments.

Based on this insight, we now consider an extended class of test profiles:

$$\phi(z) = \begin{cases} \frac{1}{2}(1-p) + p\,z - \frac{1}{2}(1-p)\left(1 - z/\delta\right)^n & \text{for} \quad 0 \leqslant z \leqslant \delta \\ \frac{1}{2}(1-p) + p\,z & \text{for} \quad \delta < z < 1-\delta \\ \frac{1}{2}(1-p) + p\,z + \frac{1}{2}(1-p)\left(1 - (1-z)/\delta\right)^n & \text{for} \quad 1-\delta \leqslant z \leqslant 1. \end{cases} \tag{5.1}$$

This class contains three independent parameters: (a) the thickness δ of the boundary segments ($0 < \delta \leqslant \frac{1}{2}$); ($b$) the profile slope p in the interior ($0 \leqslant p \leqslant 1$); ($c$) the

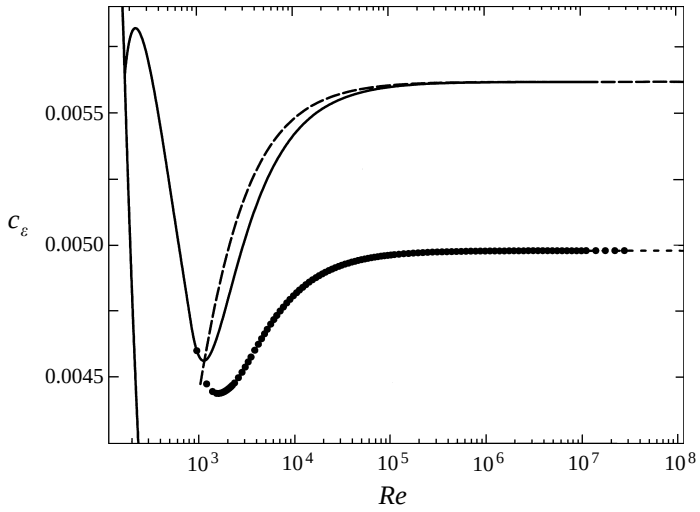

FIGURE 5. Variational bounds on $c_\varepsilon(Re)$. Solid line on the left: lower bound $\underline{c_\varepsilon}(Re) = Re^{-1}$; solid upper line: optimal upper bound provided by the test profiles (I, 4.1), cf. figure 3 of Part 1; points: improved upper bound obtained numerically with the help of the new parameter n that determines the shape of the profiles' boundary segments. The long-dashed line is the bound derived from the scaling solutions (3.7) for $n = 2$; the short-dashed line continuing the points indicates the limit (4.7).

polynomial order n of the boundary segments ($n = 2, 3, \dots$). At the matching points, these profiles are $n - 1$ times continuously differentiable. In particular, fixing $n = 2$ leads us back to the previous test profiles (I, 4.1).

The profile functional (I, 2.11), evaluated within the class (5.1), adopts the form

$$D\{\phi\} = \left[\frac{1}{2}\,\frac{n^2}{(2n-1)\,\delta} - 1\right](1-p)^2\,.$$

For each individual n the functions $\psi_{int}(z) = z$ and $\psi_{bl}(\xi) = \psi_{bl}^{(n)}(\xi)$ as defined in (4.6) provide shape functions for the test profiles (5.1). Hence, for each fixed n these profiles constitute a profile family $\phi_{\delta,p}$ that obeys for $0 \leqslant p < 1$ the specifications (i), (ii), and (iii) formulated in § 3. We therefore have scaling solutions (3.7); some values of the ensuing asymptotic upper bounds $\overline{c_\varepsilon^\infty}$ have been listed in table 1.

The overall optimal bound obtainable from the variation of all three parameters, δ, p, and n, is drawn in figure 5. We also have included the upper bound on c_ε computed previously from the profiles (I, 4.1), together with the upper bound derived from the scaling solutions (3.7) for $n = 2$, and the asymptotic bound (4.7) pertaining to the limit $n \to \infty$.

Although the improvement of the upper bound brought about by the additional variational degree of freedom is not overwhelming – the absolute minimum is shifted to slightly higher values of Re, and the asymptotic value of the bound is lowered by about 11% – it is of considerable mathematical and physical interest to investigate the new scaling behaviour of the optimal profile parameters. We can clearly distinguish three different regimes:

(*a*) For Reynolds numbers less than ≈ 975, the overall optimal upper bound is produced by the previous profile class (I, 4.1), so that in this regime the parameter n remains tied to its smallest value, $n = 2$. Consequently, the bifurcation of the wavenumbers minimizing $R_0\{\phi\}(k)$, which occurs at $Re = Re_B \approx 860$, remains un-

changed. The boundary segment thickness δ decreases monotonically with increasing Re from 0.5 to its minimal value ≈ 0.14.

(*b*) In the following regime, for $975 \lesssim Re \lesssim 2280$, we encounter a dramatic change of the shape of the boundary segments: the parameter n increases from 2 to 19, so that the internal boundary segments become steeper, while δ increases back to its maximal possible value 0.5, so that the entire boundary segments reach deeper and deeper into the bulk and finally join together. The bound on c_ε passes in this Re-regime through its minimal value $\overline{c_\varepsilon}^{min} \approx 0.443\,88 \times 10^{-2}$.

(*c*) For Re above ≈ 2280, we obtain simple scaling laws for the profile parameters: δ remains locked to the value 0.5, while n and p scale according to $n \sim aRe$, $p \sim bRe^{-1}$ in the limit of large Re, with constants a and b. This corresponds to a power-law change of the profile shape: the slope at the boundary $z = 0$ is given by

$$\phi'(0) = p + \frac{n}{2\delta}(1-p) \sim n \sim aRe,$$

whereas the slope in the middle $z = \frac{1}{2}$ becomes

$$\phi'\left(\tfrac{1}{2}\right) = p \sim bRe^{-1}.$$

The bound thus derived from the profiles (5.1) had already been included in the overview given in figure 9 of Part 1.

6. Conclusions: the principles behind the principle

Let us summarize the main results obtained in both parts of our study. Despite substantial numerical and analytical effort, it has not been possible to lower the value (I, 2.8) of the asymptotic upper bound that the Optimum Theory provides for the rate of energy dissipation in plane Couette flow (Busse 1970, 1978, 1996). In agreement with the results obtained by Kerswell (1997), the asymptotic bound (I, 6.3) derived from the extended Doering–Constantin principle coincides with Busse's number, within the uncertainty of that number.

And yet, the progress made in the present work is quite considerable. For the first time it has been possible to derive a rigorous upper bound on the dissipation rate that (i) compares favourably in the asymptotic regime with the bound given by the Optimum Theory, (ii) is free from any assumption or uncontrolled approximation whatsoever, and (iii) spans the entire range from the energy stability limit to asymptotically high Reynolds numbers. In particular, we have identified the mechanism that determines the optimal upper bound in the cross-over regime from 'low' to 'high' Reynolds numbers, namely a bifurcation of the minimizing wavenumbers, and have shown that the best asymptotic bound obtainable from the principle (I, 2.12), (I, 2.13) is approached from below.

The important technical step that has made the numerical solution of the variational principle feasible for almost arbitrary Reynolds numbers is the reformulation of its spectral constraint (I, 2.13) as an initial value problem with simple boundary condition, as outlined in § 3 of Part 1. Using this very technique, the extended Doering–Constantin principle can now routinely be applied to other problems of interest, such as channel flow or turbulent convection.

The analytical insight gained in this paper stems largely from the idea of the shape functions that specify the variational profiles separately in the interior or in the boundary layers. These shape functions have allowed us to explain the occurrence of two branches of minimizing wavenumbers quantitatively. The additional obser-

vation that the monotonic properties (3.5) suffice to guarantee the equilibration of the two minima, and thereby to bring about the numerically observed scaling behaviour of the profile parameters with the Reynolds number, even has some aesthetic appeal.

A key result of the analysis of the restricted, two-dimensional Couette problem is the variational principle (4.5) for the bound on the dissipation rate in the limit $Re \to \infty$. Numerical work indicates that this principle can be solved within the one-parameter class (4.6) of boundary layer shape functions ψ_{bl}. Hence, for all classes of variational profiles which can be described by two shape functions according to the specifications (i), (ii), and (iii) formulated in § 3, (4.7) represents the *best possible asymptotic bound* for the restricted Couette problem. This implies that, if one tries to solve the original variational principle (I, 2.12), (I, 2.13) within classes of two-shape-function profiles that are arbitrarily more sophisticated than (5.1), one should be able to improve the bound at finite Re, but not in the limit $Re \to \infty$. We conjecture that the profiles (5.1) yield the optimal asymptotic bound also for the unrestricted, three-dimensional Couette flow, and have therefore used this class of test profiles to compute the upper bound $\overline{c_\varepsilon}$ displayed in figure 8 of Part 1, even though we do not have a formal proof of this conjecture.

Although a significant step forward has been made, it must be clearly recognized that the derived bounds still lie an order of magnitude above the experimentally measured data, as shown in figure 9 of Part 1. It appears inevitable to conclude that a variational principle that is based entirely on the energy balance derived from the Navier–Stokes equations is incapable of producing bounds close to the observed experimental data. To obtain better bounds it seems necessary to formulate an advanced principle that incorporates at least some aspects of the actual dynamics.

This work was supported by the Deutsche Forschungsgemeinschaft via the Sonderforschungsbereich "Nichtlineare Dynamik", SFB 185, and by the German–Israeli-Foundation (GIF).

Appendix. Boundary value problem for rescaled profile functions with 'infinitely' extended interior

In this Appendix we evaluate the right-hand side of (2.41). To this end, we consider in a first step the system of differential equations (2.23)–(2.28) for $\xi \geqslant 0$ with arbitrary initial conditions and a constant function $\tilde{\phi}(\xi)$. For notational simplicity we write $\boldsymbol{y}(\xi)$ and $\phi(\xi)$ instead of $\tilde{\boldsymbol{y}}(\xi)$ and $\tilde{\phi}(\xi)$, respectively. The initial value problem then reads

$$\boldsymbol{y}'(\xi) = 2\kappa \boldsymbol{A}_0 \boldsymbol{y}(\xi), \quad \boldsymbol{y}(0) = \boldsymbol{y}_0; \tag{A 1}$$

$\boldsymbol{A}_0$ is defined in (2.34). With the help of the Jordan normal form $\boldsymbol{J} \equiv \boldsymbol{C}^{-1}\boldsymbol{A}_0\boldsymbol{C}$ of $\boldsymbol{A}_0$,

$$\boldsymbol{J} = \begin{pmatrix} 0 & 0 & 0 & 0 & 0 & 0 \\ 0 & -2 & 0 & 0 & 0 & 0 \\ 0 & 0 & -1 & 1 & 0 & 0 \\ 0 & 0 & 0 & -1 & 1 & 0 \\ 0 & 0 & 0 & 0 & -1 & 0 \\ 0 & 0 & 0 & 0 & 0 & -1 \end{pmatrix}, \quad \boldsymbol{C} \equiv \frac{1}{16} \begin{pmatrix} 3 & 3 & 2 & 0 & 10 & 0 \\ 3 & -3 & 0 & 2 & 0 & 0 \\ 0 & 0 & 0 & 0 & 0 & 16 \\ 3 & 3 & -2 & 0 & -6 & 0 \\ 3 & -3 & 0 & -2 & 0 & 0 \\ 3 & 3 & 2 & 0 & -6 & 0 \end{pmatrix},$$

we find the solution $\boldsymbol{y}(\xi) = \boldsymbol{Y}(\xi)\,\boldsymbol{C}^{-1}\boldsymbol{y}_0$, with

$$\boldsymbol{Y}(\xi) = \frac{1}{16}\begin{pmatrix} 3 & 3\,\mathrm{e}^{-4\kappa\xi} & 2\,\mathrm{e}^{-2\kappa\xi} & 4\kappa\xi\,\mathrm{e}^{-2\kappa\xi} & \left[10+4\kappa^2\xi^2\right]\mathrm{e}^{-2\kappa\xi} & 0 \\ 3 & -3\,\mathrm{e}^{-4\kappa\xi} & 0 & 2\,\mathrm{e}^{-2\kappa\xi} & 4\kappa\xi\,\mathrm{e}^{-2\kappa\xi} & 0 \\ 0 & 0 & 0 & 0 & 0 & 16\,\mathrm{e}^{-2\kappa\xi} \\ 3 & 3\,\mathrm{e}^{-4\kappa\xi} & -2\,\mathrm{e}^{-2\kappa\xi} & -4\kappa\xi\,\mathrm{e}^{-2\kappa\xi} & -\left[6+4\kappa^2\xi^2\right]\mathrm{e}^{-2\kappa\xi} & 0 \\ 3 & -3\,\mathrm{e}^{-4\kappa\xi} & 0 & -2\,\mathrm{e}^{-2\kappa\xi} & -4\kappa\xi\,\mathrm{e}^{-2\kappa\xi} & 0 \\ 3 & 3\,\mathrm{e}^{-4\kappa\xi} & 2\,\mathrm{e}^{-2\kappa\xi} & 4\kappa\xi\mathrm{e}^{-2\kappa\xi} & \left[-6+4\kappa^2\xi^2\right]\mathrm{e}^{-2\kappa\xi} & 0 \end{pmatrix}.$$

Note that the largest eigenvalue of $\boldsymbol{A}_0$ is zero. Therefore, all columns of $\boldsymbol{Y}(\xi)$ except for the first are exponentially damped (since $\kappa > 0$); the first column is an eigenvector of $\boldsymbol{A}_0$ belonging to the eigenvalue zero. As a consequence, the solution $\boldsymbol{y}(\xi)$ approaches a constant vector proportional to this eigenvector in the limit of large ξ,

$$\lim_{\xi\to\infty}\boldsymbol{y}(\xi) = \frac{3}{16}\left[\boldsymbol{C}^{-1}\boldsymbol{y}_0\right]_1\boldsymbol{e}_0, \tag{A 2}$$

where $\boldsymbol{e}_0 \equiv (1,1,0,1,1,1)^T$, and $\left[\boldsymbol{C}^{-1}\boldsymbol{y}_0\right]_1$ denotes the first component of the vector $\boldsymbol{C}^{-1}\boldsymbol{y}_0$.

We now formulate two different eigenvalue problems that refer to the shape functions $\psi_{bl}(\xi)$ introduced in § 2.2. For a given ψ_{bl} with the properties (2.37) and (2.38), both eigenvalue problems are based on the system of differential equations (2.23)–(2.28),

$$y_1' = 2\kappa\left[-y_1 + y_2\right], \tag{A 3}$$
$$y_2' = 2\kappa\left[\tfrac{1}{2}y_1 - y_2 + \tfrac{1}{2}y_4\right], \tag{A 4}$$
$$y_3' = -2\kappa y_3 - \frac{\sigma}{\kappa}\,\psi_{bl}'\,y_1, \tag{A 5}$$
$$y_4' = 2\kappa\left[-y_4 + y_5\right], \tag{A 6}$$
$$y_5' = 2\kappa\left[\tfrac{1}{4}y_1 + \tfrac{1}{2}y_4 - y_5 + \tfrac{1}{4}y_6\right], \tag{A 7}$$
$$y_6' = 2\kappa\left[y_2 - y_6\right] + \frac{\sigma}{2\kappa}\,\psi_{bl}'\,y_3. \tag{A 8}$$

The first eigenvalue problem is defined by integrating this system from 0 to $\frac{1}{2}$ with initial values (2.29),

$$\boldsymbol{y}(0) = (0,0,0,0,0,1)^T, \tag{A 9}$$

and boundary condition

$$\left[\boldsymbol{C}^{-1}\boldsymbol{y}\left(\tfrac{1}{2}\right)\right]_1 = 0. \tag{A 10}$$

With κ and ψ_{bl} as input, we search for the smallest positive value of σ which solves this boundary value problem, denoted as $\sigma^{(1)}\{\psi_{bl}\}(\kappa)$.

The second eigenvalue problem is defined by integrating the system from $\frac{1}{2}$ to 1 with initial values (2.42),

$$\boldsymbol{y}\left(\tfrac{1}{2}\right) = (1,1,0,1,1,1)^T = \boldsymbol{e}_0, \tag{A 11}$$

and boundary condition (2.43),

$$y_1(1) = 0. \tag{A 12}$$

Again we search for the smallest positive value of σ which solves this boundary value problem, denoted as $\sigma^{(2)}\{\psi_{bl}\}(\kappa)$.

From the previous discussion it is clear that if one glues the left-hand boundary segment of $\psi_{bl}(\xi)$ at $\xi = \frac{1}{2}$ to the constant function defined by $\psi(\xi) = \frac{1}{2}$ for $\xi > \frac{1}{2}$,

takes the result as an input to the system (A 3)–(A 8), and integrates it with initial condition (A 9), then the choice $\sigma = \sigma^{(1)}$ ensures that the solution vector vanishes in the limit $\xi \to \infty$, since (A 10) sets the prefactor of $\boldsymbol{e}_0$ to zero, cf. (A 2). On the other hand, the integration of the second problem starts with this eigenvector, so that for $\sigma = \sigma^{(2)}$ the usual boundary condition posed at the end of the right-hand boundary layer is satisfied. We remark that we do not want to treat the mathematically non-trivial questions concerning the precise properties of the functions ψ_{bl} that can guarantee the existence of the required values $\sigma^{(1)}$ and $\sigma^{(2)}$, but rather we assume that ψ_{bl} is chosen appropriately.

Returning to the evaluation of the right-hand side of (2.41), we observe that

$$\lim_{\delta \to 0} \rho_0\{\psi\}(\kappa) = \min\left\{\sigma^{(1)}\{\psi_{bl}\}(\kappa), \sigma^{(2)}\{\psi_{bl}\}(\kappa)\right\}. \tag{A 13}$$

Namely, in order to determine ρ_0 we have to integrate the system (2.23)–(2.28) with ψ as input, see (2.39), and make sure that the boundary condition (2.30) is satisfied. When letting δ tend to zero, so that the length of the interior segment of ψ tends to infinity, we are faced with the following alternative at the merging point to the right-hand boundary layer: either the solution vector vanishes, since the prefactor of $\boldsymbol{e}_0$ is zero, and consequently the solution will remain the zero-vector in the right-hand boundary layer, or the solution vector is proportional to $\boldsymbol{e}_0$. In the first case the eigenvalue ρ_0 is by construction equal to $\sigma^{(1)}$, in the second case equal to $\sigma^{(2)}$. Inverting this argument, if $\sigma^{(1)}$ and $\sigma^{(2)}$ have been determined from their eigenvalue problems, two candidates for $\lim_{\delta \to 0} \rho_0$ have been found. Since ρ_0 is defined as the smallest positive eigenvalue, (A 13) follows. In the rest of this Appendix we will show that $\sigma^{(1)}$ and $\sigma^{(2)}$ are actually equal.

To create a link between the two eigenvalue problems, we have to consider a third one. For a given shape function ψ_{bl} we take an ϵ with $-1 < \epsilon < 1$, and define the function

$$\psi_\epsilon(\xi) \equiv \begin{cases} (1+\epsilon)\,\psi_{bl}(\xi) & \text{for} \quad 0 \leqslant \xi \leqslant \frac{1}{2} \\ \frac{1}{2}(1+\epsilon) & \text{for} \quad \frac{1}{2} < \xi < \ell + \frac{1}{2} \\ 1 - (1-\epsilon)\,\psi_{bl}(\ell + 1 - \xi) & \text{for} \quad \ell + \frac{1}{2} \leqslant \xi \leqslant \ell + 1. \end{cases}$$

This function equals $\psi(\xi)$ as introduced in (2.39), if we set $\epsilon = 0$ and $\ell = (2\delta)^{-1} - 1$. Note that ϵ plays the role of an asymmetry parameter: the constant interior segment is shifted by an amount $\epsilon/2$ with respect to the previous value $\frac{1}{2}$. Such a shift will turn out to be the key for connecting the eigenvalues $\sigma^{(1)}$ and $\sigma^{(2)}$.

Our third eigenvalue problem again arises from the system (A 3)–(A 8), but now considered in the interval $[0, \ell + 1]$, and the input function ψ_{bl} is replaced by ψ_ϵ. The initial values (A 9) are supplemented by the boundary condition $y_1(\ell + 1) = 0$. The smallest positive eigenvalue σ will now be written as $\sigma_\ell\{\psi_{bl}\}(\epsilon, \kappa)$.

At this point we resort to a symmetry property of the actual physical problem, namely the point symmetry with respect to $\left(x = 0, z = \frac{1}{2}\right)$. This symmetry manifests itself in the fact that the spectra of the eigenvalue problem (I, 2.13) for some fixed R and two different functions $\phi_1(z)$ and $\phi_2(z)$ are identical, if both functions are continuously differentiable and satisfy the boundary conditions at $z = 0$ and $z = 1$, and are related by $\phi_2(z) = 1 - \phi_1(1 - z)$. It is not required that the two functions obey the profiles' symmetry condition. Since σ_ℓ corresponds to the passage of the lowest eigenvalue through zero, and since the differential equations depend only on the absolute value of the wavenumber, the relation $\psi_{-\epsilon}(\xi) = 1 - \psi_\epsilon(\ell + 1 - \xi)$ leads

to the key equation

$$\sigma_\ell\{\psi_{bl}\}(\epsilon,\kappa) = \sigma_\ell\{\psi_{bl}\}(-\epsilon,\kappa)\,. \tag{A 14}$$

Taking $\lim_{\ell\to\infty}\sigma_\ell\{\psi_{bl}\}(\epsilon,\kappa) \equiv \sigma_\infty\{\psi_{bl}\}(\epsilon,\kappa)$, (A 14) yields

$$\sigma_\infty\{\psi_{bl}\}(\epsilon,\kappa) = \sigma_\infty\{\psi_{bl}\}(-\epsilon,\kappa)\,. \tag{A 15}$$

We can now formulate the

LEMMA. Let $\psi_{bl}(\xi)$ be a shape function for the boundary layers. Then we have for all $\kappa > 0$ the identity

$$\sigma^{(1)}\{\psi_{bl}\}(\kappa) = \sigma^{(2)}\{\psi_{bl}\}(\kappa)\,. \tag{A 16}$$

Proof. For each shape function $\psi_{bl}(\xi)$, rescaled wavenumber $\kappa > 0$, and ϵ taken from the interval $(-1,1)$, we define $\tilde{\sigma}^{(1)}\{\psi_{bl}\}(\epsilon,\kappa)$ as the smallest positive value of σ for which the boundary value problem posed by (A 3)–(A 8) with $\psi_{bl}(\xi)$ replaced by $(1+\epsilon)\,\psi_{bl}(\xi)$, initial values (A 9), and boundary value (A 10) is solved. Likewise, let $\tilde{\sigma}^{(2)}\{\psi_{bl}\}(\epsilon,\kappa)$ be the smallest positive value of σ for which the boundary value problem posed by (A 3)–(A 8) with $\psi_{bl}(\xi)$ replaced by $1-(1-\epsilon)\,\psi_{bl}(1-\xi)$, initial values (A 11), and boundary value (A 12) is satisfied. Because the system (A 3)–(A 8) depends on σ only through the product $\sigma\psi'_{bl}(\xi)$, we obtain

$$\tilde{\sigma}^{(1)}\{\psi_{bl}\}(\epsilon,\kappa) = \frac{1}{1+\epsilon}\,\sigma^{(1)}\{\psi_{bl}\}(\kappa)\,,$$

$$\tilde{\sigma}^{(2)}\{\psi_{bl}\}(\epsilon,\kappa) = \frac{1}{1-\epsilon}\,\sigma^{(2)}\{\psi_{bl}\}(\kappa)\,.$$

In analogy to the preceding discussion we deduce

$$\lim_{\ell\to\infty}\sigma_\ell\{\psi_{bl}\}(\epsilon,\kappa) = \sigma_\infty\{\psi_{bl}\}(\epsilon,\kappa) = \min\left\{\tilde{\sigma}^{(1)}\{\psi_{bl}\}(\epsilon,\kappa)\,,\tilde{\sigma}^{(2)}\{\psi_{bl}\}(\epsilon,\kappa)\right\}.$$

Thus, (A 15) produces the equation

$$\min\left\{\frac{1}{1+\epsilon}\,\sigma^{(1)}\{\psi_{bl}\}(\kappa)\,,\frac{1}{1-\epsilon}\,\sigma^{(2)}\{\psi_{bl}\}(\kappa)\right\} = \min\left\{\frac{1}{1-\epsilon}\,\sigma^{(1)}\{\psi_{bl}\}(\kappa)\,,\frac{1}{1+\epsilon}\,\sigma^{(2)}\{\psi_{bl}\}(\kappa)\right\}. \tag{A 17}$$

If we now assume that $\sigma^{(1)} \neq \sigma^{(2)}$, we may stipulate without loss of generality that $\sigma^{(1)} < \sigma^{(2)}$. Then we choose $0 < \epsilon < 1$ such that

$$\frac{1}{1-\epsilon}\,\sigma^{(1)}\{\psi_{bl}\}(\kappa) < \frac{1}{1+\epsilon}\,\sigma^{(2)}\{\psi_{bl}\}(\kappa)\,,$$

and conclude from (A 17)

$$\frac{1}{1+\epsilon}\,\sigma^{(1)}\{\psi_{bl}\}(\kappa) = \frac{1}{1-\epsilon}\,\sigma^{(1)}\{\psi_{bl}\}(\kappa)\,.$$

This equation requires $\sigma^{(1)} = 0$, which contradicts the proposition $\sigma^{(1)} > 0$. Hence, we necessarily have $\sigma^{(1)} = \sigma^{(2)}$. □

Applying this lemma to (A 13), we finally obtain

$$\lim_{\delta\to 0}\rho_0\{\psi\}(\kappa) = \sigma^{(1)}\{\psi_{bl}\}(\kappa) = \sigma^{(2)}\{\psi_{bl}\}(\kappa)\,. \tag{A 18}$$

By definition, $\sigma^{(2)}\{\psi_{bl}\}(\kappa)$ is identical to $\sigma_0\{\psi_{bl}\}(\kappa)$ as employed in § 2.2.

REFERENCES

Busse, F. H. 1970 Bounds for turbulent shear flow. *J. Fluid Mech.* **41**, 219–240.

Busse, F. H. 1978 The Optimum Theory of turbulence. *Adv. Appl. Mech.* **18**, 77–121.

Busse, F. H. 1996 Bounds for properties of complex systems. In *Nonlinear Physics of Complex Systems — Current Status and Future Trends* (ed. J. Parisi, S. C. Müller & W. Zimmermann). Lecture Notes in Physics, vol. 476, pp. 1–9. Springer.

Doering, C. R. & Constantin, P. 1994 Variational bounds on energy dissipation in incompressible flows: shear flow. *Phys. Rev.* E **49**, 4087–4099.

Kerswell, R. R. 1997 Variational bounds on shear-driven turbulence and turbulent Boussinesq convection. *Physica* D **100**, 355–376.

Nicodemus, R. 1997 Rigorous bounds on energy dissipation in turbulent shear flow. PhD thesis, Universität Marburg (http://archiv.ub.uni-marburg.de/diss/dissmain.html).

Nicodemus, R., Grossmann, S. & Holthaus, M. 1997*a* Improved variational principle for bounds on energy dissipation in turbulent shear flow. *Physica* D **101**, 178–190.

Nicodemus, R., Grossmann, S. & Holthaus, M. 1997*b* Variational bound on energy dissipation in plane Couette flow. *Phys. Rev.* E **56**, 6774–6786.

Nicodemus, R., Grossmann, S. & Holthaus, M. 1998 The background flow method. Part 1. Constructive approach to bounds on energy dissipation. *J. Fluid Mech.* **363**, 281–300.